# Supporting information

## Giant Enhancement of Second-Harmonic Generation in Indium Selenide on Planar Au

Yuxuan Ke,[†] Chun Li,[†] Yin Liang,[†] Xi Zhang, Jiepeng Song,[†] Ruijie Li,[†] Lei Liu,[†] Junfeng Dai, Zhongming Wei,[§] Qing Zhang.[†,*]

[†]School of Materials Science and Engineering, Peking University, Beijing 100871, China

[ʃ]Southern University of Science and Technology, Shenzhen, 518055, China

[§]State Key Laboratory of Superlattices and Microstructures, Institute of Semiconductors, Chinese Academy of Sciences, Beijing 100083, China

[*]Corresponding: Q_zhang@pku.edu.cn

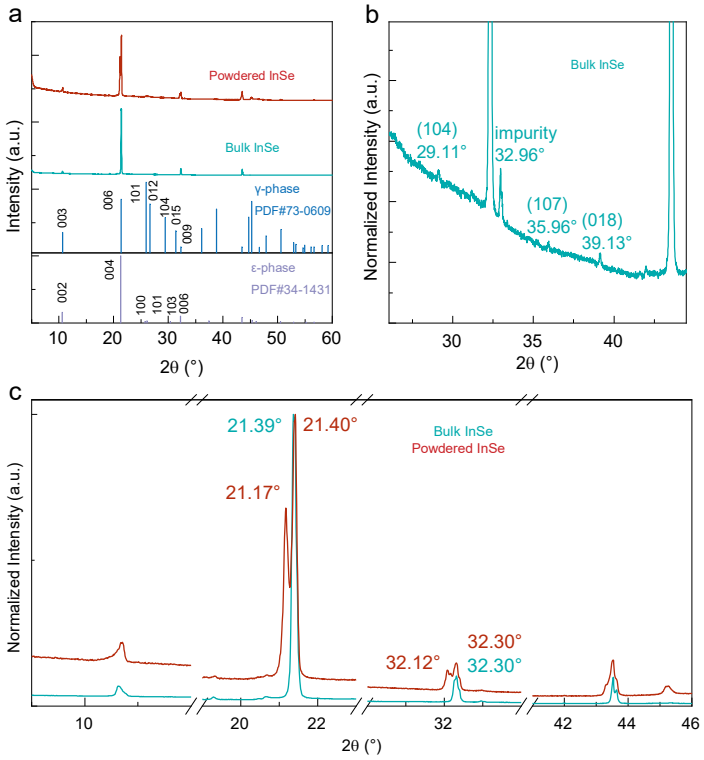


**Fig. S1** (a) XRD patterns of the bulk (cyan) and powdered (red) InSe. (b) The zoomed-in XRD pattern of the bulk InSe with the large angle range. (c) The zoomed-in XRD patterns of the bulk and powdered InSe at these peaks of 21.39° and 32.3°.

To confirm the phase of InSe in our work, the X-ray diffraction (XRD) patterns of the bulk and powdered InSe by grinding were performed in Fig. S1a. Fig. S1b shows that these peaks of 29.11°, 35.96° and 39.13° match with the standard data file PDF 73-0609, corresponding to (104), (107) and (018) planes of $\gamma$-InSe. Meanwhile, in comparison of XRD patterns of bulk and powdered InSe (Fig. S1c), these two peaks (21.39° and 32.30°) of bulk InSe correspond to the (006) and (009) planes of $\gamma$-InSe. However, two splitting peaks (21.17° and 32.12°) of powdered InSe correspond to the (004) and (006) planes of $\varepsilon$-InSe. Layer gliding during the grinding process could result in the formation of $\varepsilon$-phase in $\gamma$-phase powered InSe, and thus the peak splitting.[1] These indicate that the InSe in our work is $\gamma$-phase.

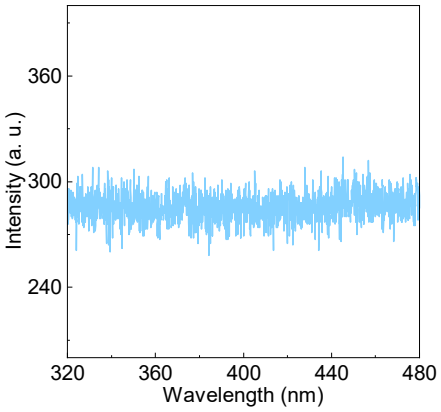


**Fig. S2** The SHG spectrum of Au film with no obvious signal. The excitation wavelength is 800 nm with the power is 1 mW, and the integration time is 1 s.

**Fig. S3** (a) As-fabricated InSe/h-BN/Au hybrid structure where InSe is 33 nm and h-BN is 7 nm. The scale bar is 50 μm. (b) SHG spectrum of h-BN on Au. SHG intensities of InSe on Au and h-BN/Au substrates under wavelength excitation of 800 nm with moderate (c) and high (d) power densities of $1.6\times10^{8}$ and $8.1\times10^{8}$ mW/cm$^{2}$, respectively. Ten groups of data are

measured on the same position. The lateral-view excitation electric field distributions of 33-nm-thick InSe on Au (e) and h-BN/Au (f), respectively, with excitation wavelength of 800 nm.

Fig. S3a shows an as-fabricated InSe/h-BN/Au hybrid structure where InSe is 33 nm and h-BN is 7 nm. The exfoliated h-BN was firstly transferred onto $SiO_2$ with Au film patterns, making one part of h-BN located on the top of Au film and another on the top of $SiO_2$ substrate. The exfoliated InSe was transferred on h-BN/Au, making the one part of InSe on the top of h-BN/Au and another on the top of Au. To research the effect of charge transfer on SHG of InSe on Au, the InSe/h-BN/Au hybrid structure can be designed as a control experiment and h-BN is as a block layer of charge transfer. Fig. S3c displays SHG intensity distributions of InSe on Au and h-BN/Au under excitation wavelength of 800 nm with moderate power density of $1.6\times10^8$ mW/cm$^2$. The average intensity of InSe on h-BN/Au is approximately 1.4-fold larger than that on Au. The contribution of h-BN SHG can be excluded as no obvious SHG signal can be observed in Fig. S3b due to even number of layers with inversion symmetry.[2] Figs. S3e and S3f show that according to calculated electric field distributions by finite-differences time-domain, the $|E|^4$ of InSe on h-BN/Au is enhanced by approximately 2.0-fold compared to that on Au. This indicates that the SHG enhancement of InSe on h-BN/Au is attributed to the electric field enhancement, and charge transfer have little fluence on the SHG intensity for the InSe/Au structure. For high power density of $8.1\times10^8$ mW/cm$^2$, however, the average intensity of InSe on h-BN/Au is approximately 1.1-fold larger than that on Au (Fig. S3d), indicating that the charge transfer generates the significant influence on the SHG for InSe/Au structure.

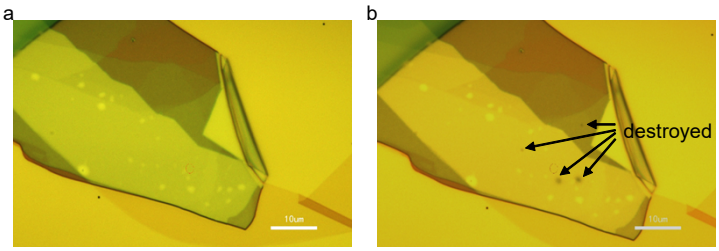


**Fig. S4** The optical images of InSe (32 nm) on Au substrate before (a) and after (b) measurement using the high excitation density of $1.1\times10^9$ mW cm$^{-2}$.

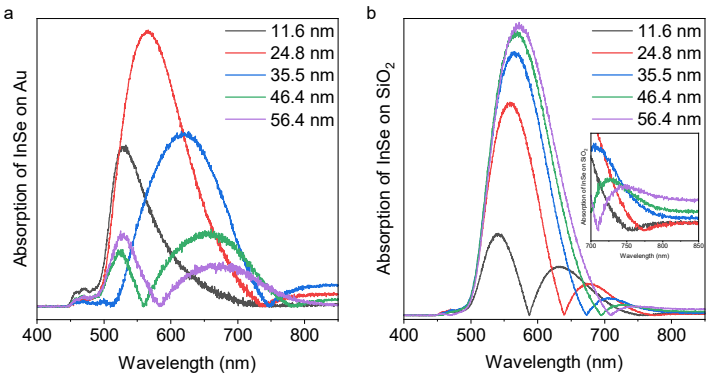


**Fig. S5** Absorptions of InSe with 11.6, 24.8, 35.5, 46.4 and 56.4 nm thickness for InSe-Au (a) and InSe-$SiO_2$ (b) structures; inset is the zoomed-in absorption spectrum of InSe on $SiO_2$ substrate (b) from 700 to 850 nm. The absorption is defined as $A = \frac{R_{Substrate} - R_{InSe}}{R_{Substrate}}$, where $A$ is the absorption within InSe for InSe-Au and InSe-$SiO_2$ structures, and $R_{\mathrm{Substrate}}$ and $R_{\mathrm{InSe}}$ are reflection spectra of Au/$SiO_2$ and InSe on Au/$SiO_2$, respectively.

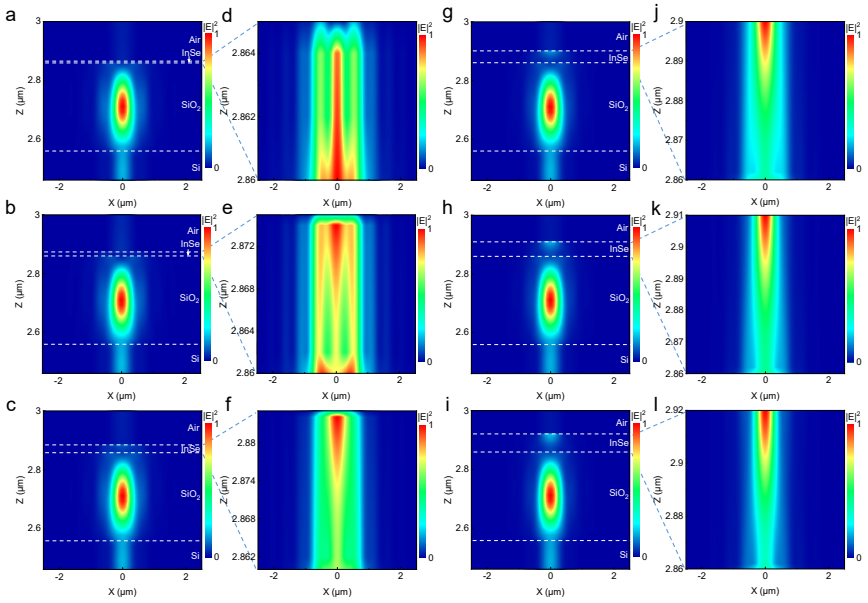


**Fig. S6** The lateral-view excitation electric field distributions of InSe on $SiO_2$ with different thickness. The lateral-view excitation electric field distribution of InSe on $SiO_2$ with 5 (a), 15 (b), 25 (c), 40 (g), 50 (h) and 60 nm (i), respectively. (d-f, j-l) corresponding zoomed-in electric field distributions of InSe. The excitation wavelength is 800 nm.

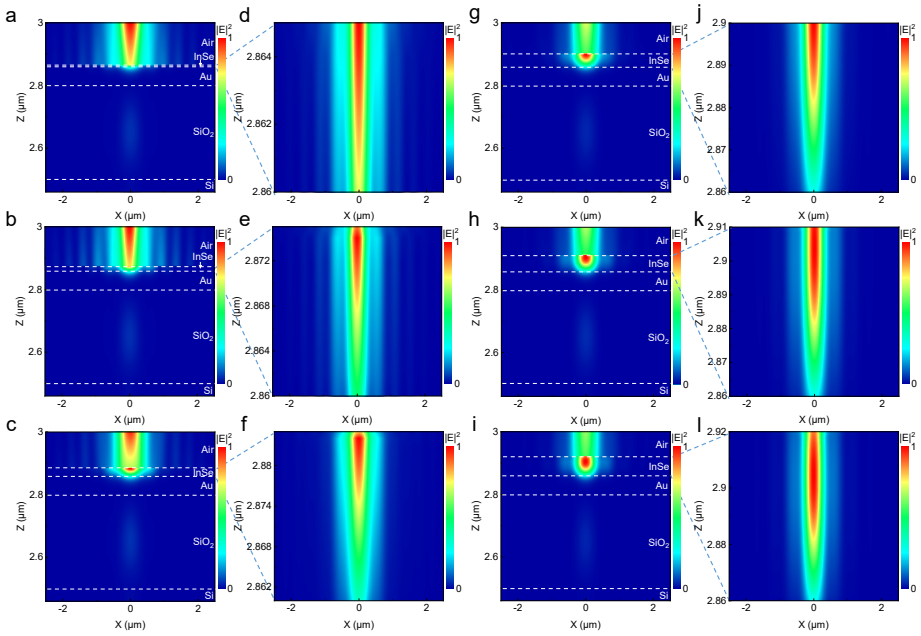


**Fig. S7** The lateral-view excitation electric field distributions of InSe on Au with different thickness. The lateral-view excitation electric field distribution of InSe on Au with 5 (a), 15 (b), 25 (c), 40 (g), 50 (h) and 60 nm (i), respectively. (d-f, j-l) corresponding zoomed-in electric field distributions of InSe. The excitation wavelength is 800 nm.

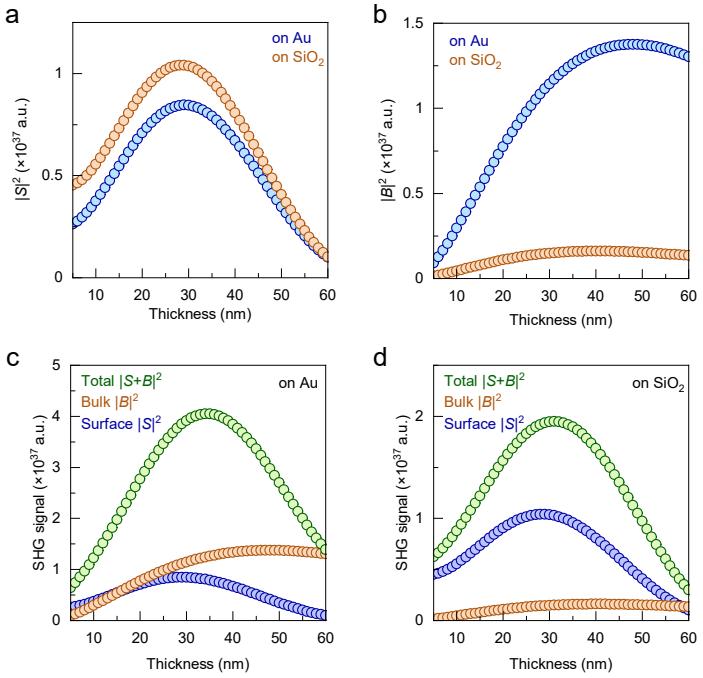


**Fig. S8** Reflection simulation of InSe on Au and $SiO_2$, respectively, as a function of thickness. (a, b) $|S|^2$ and $|B|^2$ SHG contributions of InSe on Au (blue) and $SiO_2$ (orange), respectively, as

functions of $H$. (c-d) $|S|^2$ (blue), $|B|^2$ (orange), and $|S+B|^2$ (green) SHG contributions of InSe on Au and $SiO_2$, respectively, as a function of $H$.

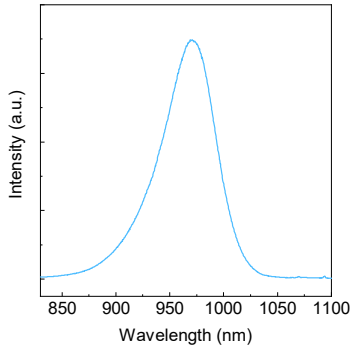


**Fig. S9** The PL spectrum of InSe with ≈30 nm thickness under 532 nm excitation with the power of 1.5 mW. The peak is 970 nm.

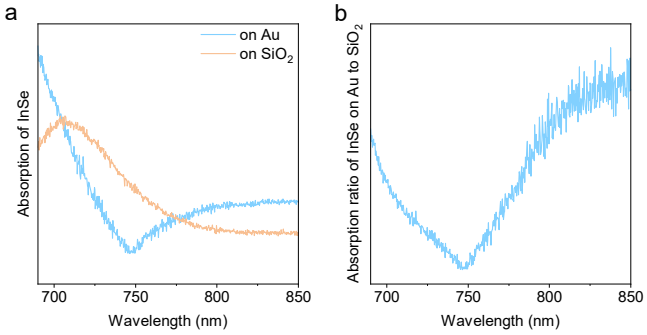


**Fig. S10** (a) Absorption spectra of 35.5 nm-InSe on Au and $SiO_2$ substrates from 690 to 850 nm; (b) the absorption ratio of InSe on Au to $SiO_2$.

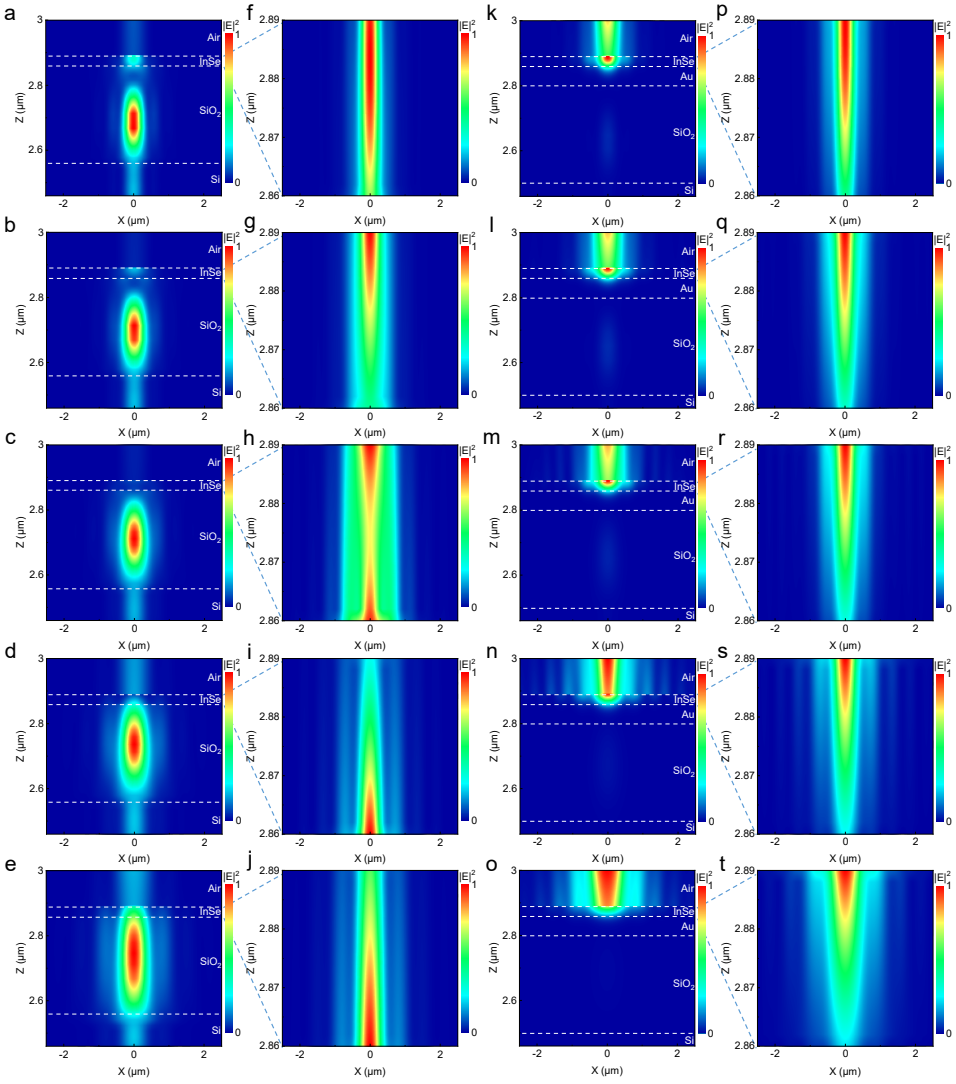


**Fig. S11** The lateral-view excitation electric field distributions of 30-nm-thick InSe on $SiO_2$ and Au, respectively, with different excitation wavelengths. The lateral-view excitation electric field distributions of 30-nm-thick InSe on $SiO_2$ (a-e) and Au (k-o), respectively, with 690, 750, 820, 940, and 1060 nm. (f-j, p-t) corresponding zoomed-in electric field distributions of InSe on $SiO_2$ and Au, respectively.

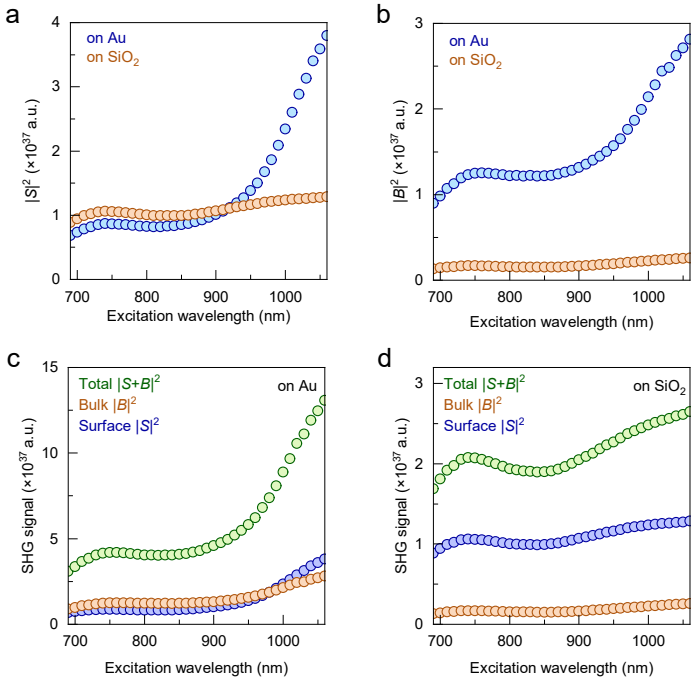


**Fig. 12** SHG Reflection simulation of InSe on Au and $SiO_2$, respectively, as a function of excitation wavelength. (a-b) $|S|^2$ and $|B|^2$ SHG contributions of InSe on Au (blue) and $SiO_2$ (orange), respectively, as functions of excitation wavelength. (c-d) $|S|^2$ (blue), $|B|^2$ (orange), and $|S+B|^2$ (green) SHG contributions of InSe on Au and $SiO_2$, respectively, as a function of excitation wavelength.

**Note S1.** Theory model

This model is used to explain the interference between surface and bulk SHG without considering phase mismatch from the bulk contribution of SHG. In this model, a geometry consisting of three layers is considered: air (layer 0), InSe (layer 1) and the $SiO_2$ (or Au) substrate (layer 2) where $n_0$, $N_1$ (  ) = $n_1$ (  ) + $ik_1$ (  ) and $N_2$ (  ) = $n_2$ (  ) + $ik_2$ (  ). For the index of air, the imaginary part is assumed as zero due to negligible weak light absorption. The total second harmonic intensity as a function of the InSe thickness can be written as:[3, 4]

$$I_{SHG}(L) = \frac{32\pi^3\omega^2}{c^3 n_1(\omega) n_1(2\omega)} \left| S(L) + B(L) \right|^2 I_0^2$$

where $L$ is the thickness of InSe, $S$ is the contributions from the top and bottom surface SHG, $B$ is the contribution from bulk SHG, and $I_0$ is the intensity of excited light. For simplicity, two first SHG contributions of the multiple reflections are only considered in the calculations of $S(L)$ and $B(L)$. Therefore,

$$S(L) = \chi_s^{(2)} \left( R_{01} + T_{01} T_{10} R_{12} e^{2iKL} + t_{10}{}^2 R_{12} T_{10} e^{2ikL} e^{iKL} \right)$$

and

$$B(L) = \chi_b^{(2)} L \left( T_{10} t_{10}{}^2 R_{12} e^{2iKL} + t_{10}{}^2 r_{12}{}^2 T_{10} e^{2ikL} e^{iKL} \right)$$

where $r_{ij} = \frac{n_i - n_j}{n_i + n_j}$, $t_{ij} = \frac{2n_i}{n_i + n_j}$ are the Fresnel coefficients at the excited wavelength $\lambda$, and $R_{ij} = \frac{n_i - n_j}{n_i + n_j}$, $T_{ij} = \frac{2n_i}{n_i + n_j}$ at the second harmonic wavelength $\lambda_2$. $k = \frac{2\pi N_1(\omega)}{\lambda_\omega}$ and $K = \frac{2\pi N_1(2\omega)}{\lambda_{2\omega}}$ are the wave vectors at the excited and second harmonic wavelengths, respectively. $\chi_s^{(2)}$ is the second-order sheet polarizability for InSe surfaces, and $\chi_b^{(2)}$ is the second-order nonlinear susceptibility for the InSe bulk.

References


1 T.-R. Wei, M. Jin, Y. Wang, H. Chen, Z. Gao, K. Zhao, *et al.*, Exceptional plasticity in the bulk single-crystalline van der Waals semiconductor InSe, *Science*, 2020, **369**(6503), 542-545.

2 Y. Li, Y. Rao, K. F. Mak, Y. You, S. Wang, C. R. Dean, *et al.*, Probing Symmetry Properties of Few-Layer $MoS_2$ and h-BN by Optical Second-Harmonic Generation, *Nano Lett.*, 2013, **13**(7), 3329-3333.

3 J. Shi, P. Yu, F. Liu, P. He, R. Wang, L. Qin, *et al.*, 3R $MoS_2$ with Broken Inversion Symmetry: A Promising Ultrathin Nonlinear Optical Device, *Adv. Mater.*, 2017, **29**(30), 1701486.

4 B. Koopmans, A. Anema, H. T. Jonkman, G. A. Sawatzky, F. van der Woude, Resonant-Optical-Second-Harmonic Generation from Thin $C_{60}$ Films, *Phys. Rev. B*, 1993, **48**(4), 2759-2764.